On Projection of Safe Operation for Grid-Following Inverters – Grid Parameter Estimation

Tareq Hossen
Department of Electrical and Computer Engineering
Kansas State University
Manhattan, KS, USA
thossen@ksu.edu

Behrooz Mirafzal
Department of Electrical and Computer Engineering
Kansas State University
Manhattan, KS, USA
mirafzal@ksu.edu

***Abstract*– This work investigates the projection of safe operation for grid-following inverters using a reference model. This work applies recursive-least square and model reference adaptive estimation techniques to estimate the unknown grid parameters. The estimated grid parameters are used in a dynamic reference model to project the safe operation of the inverter. This work also demonstrates that the controller nonlinearity and parameter variations can cause unsafe operations, such as unexpected instability at low power levels, namely hidden mode of instability. This instability issue in the nominal operating range may occur for given control parameters in a weak-grid condition. The dynamic reference model for PQ-controlled inverters is applied to analyze this instability issue using the estimated grid parameters. Both adaptive identification techniques can estimate the unknown parameters accurately, and the dynamic reference model can safeguard inverters from an unsafe operation, i.e., hidden instability, by examining the incoming new power setpoints before engaging them to the local controller. The findings are experimentally verified using a small-scale two-level 208 V, 5 kVA inverter feeding a 12 kW NHR 9410 power grid emulator.**

***Index Terms* –Grid-following inverters, Grid parameter estimation, reference model, weak grid, recursive-least square, model reference adaptive estimation**

I. INTRODUCTION

A smart cyber-physical device, i.e., a smart inverter, provides controllable and interactive interfaces between the cyber network and physical devices using communication links. These interfaces allow autonomous and bi-directional information exchange between the parties while performing proactive actions [1]-[3]. For instance, a smart inverter can operate in different modes of operation, such as grid-supporting mode when voltage regulation and harmonic compensation are accomplished while overcoming various instability issues and grid-forming mode when networked microgrid operation with black-start capabilities can be achieved [4]-[6]. Inverters need to identify some of the system's unknown parameters for implementing these advanced control features, which can be measured, projected, or acknowledged externally from adjacent smart devices. To achieve these, the inverter needs to communicate with several parties that impose more surface for detrimental events. The possibilities of harmful events increase when unsafe communication protocols are employed, and obsolete operating systems are involved [7]-[10].

Insecure incidents can exist in the form of intentional or unintentional unsafe events or naturally happened anomalies in the system, i.e., a malfunction in a physical system. For example, an authorized operator can accidentally send unsafe setpoints that can move the inverter operating point from a stable region to an unstable one, causing undesired power oscillation below the rated power level and jeopardizing the inverter's safe operation. Alternatively, an unauthorized user can purposefully alter the measurement data received from an external sensor. Notably, the inverters' low or zero inertia characteristics are more susceptible to instantaneous changes and can quickly lead to an undesired power oscillation of the power grid, mainly when the grid is weak [11]-[13]. The risk of having unsafe operations of inverters can increase more when multiple inverters are operating in a system and occupied with the same communication channel along with the other adjacent smart devices. Therefore, security actions are essential to detect and prevent anomalies in the system to sustain safe system operation.

Several investigations have been reported in the literature to ensure the safe operation of the inverter under abnormal conditions. Self-security algorithms based on a reference model have been developed [14] to examine the data and perform critical protective decisions before utilizing the incoming information in the local controller. For the implementation of any reference model, the inverter must learn about the input and output circuits to determine its normal operating region by estimating system parameters. For the grid-following inverters, unknown grid parameters are required to estimate in real-time to develop analytical reference models as described in [15]-[16]. In the literature, several methods are proposed for online grid-parameter estimation. Online grid parameter estimation techniques can be broadly classified as active and passive types [17]-[19]. In passive grid parameter estimation methods, the existing disturbance present in power networks is used [20]. Some notable passive methods are described in [21]. However, passive methods have some problems in experimental grid parameters estimation due to the lack of information. Active grid parameter estimation methods inject a disturbance into the grid or distributed generation network for parameter estimation. In this paper, two different grid parameter estimation technique has been implemented, and a comparison is performed.

This paper contains four more sections. Section II presents the system description and modeling where different online grid parameter estimation techniques are implemented. Section III elaborates on different grid parameter estimation algorithms. Section IV presents the experimental results. Finally, the paper is concluded in section V.

II. System Description and Modeling

The schematic diagram of the PQ-controlled grid-following inverter is depicted in Fig. 1. As shown in Fig. 1 inverter is equipped with an *LCL* filter and a PQ controller. The grid is represented by an equivalent grid inductance, L_g, a resistance, R_g, and a grid voltage, v_g. The voltage and current sensors are located after the *LCL* filter at PCC. The measured voltages and currents at PCC are converted to the dq-frame, which is used as inputs to the PQ-control scheme. Both P and Q controller has two cascaded loops consisting of outer power and inner current control loops. To generate the reference signal for the PWM generator, the outputs of the PQ controller, v_q^{inv} and v_d^{inv}, are utilized, see Fig. 1. Herein, v_c is the filter capacitor voltage, the state variable of the outer control loop and inner control loop are y_1, and y_2 respectively. The PQ-controlled inverter operation is not linear for two reasons. First, measured P and Q are used by the P and Q control loops are nonlinear equations. In the synchronously rotating dq reference frame locked at PCC, i.e. $v_d^{pcc} = 0$, the active and reactive power can represent as $P = (3/2)(v_q^{pcc} i_q)$ and $Q = (3/2)(v_q^{pcc} i_d)$, where, v_q^{pcc} is the amplitude of the line-line voltage at PCC, and i_q and i_d represent the line currents in dq-frame [10].]. The linearized power equations around a steady-state operating point can be represented as; $P = (3/2)\left(V_{qo}^{pcc} i_q + I_{qo} v_q^{pcc}\right)$ and $Q = (3/2)\left(V_{qo}^{pcc} i_d + I_{do} v_q^{pcc}\right)$, where, V_{qo}^{pcc} is the q-axis operating voltage, I_{do} represents the d-axis operating currents and I_{qo} represents the q-axis operating currents. I_{qo} and I_{do} will appear in the inverter closed-loop model shown in (1). Therefore, eigenvalues of the closed-loop model are a function of P and Q. The details of the closed-loop model can be obtained from [22]-[23]. Considering the operating point currents, i.e., I_{qo} and I_{do}, in this full-order model, the nonlinear operation of the inverter can be predicted, which can prevent the inverter from an unsafe operation. For the implementation of the inverter full-order model as a dynamic reference model to project the safe operation of the inverter for incoming power setpoints, the unknown grid parameters are required to estimate online.

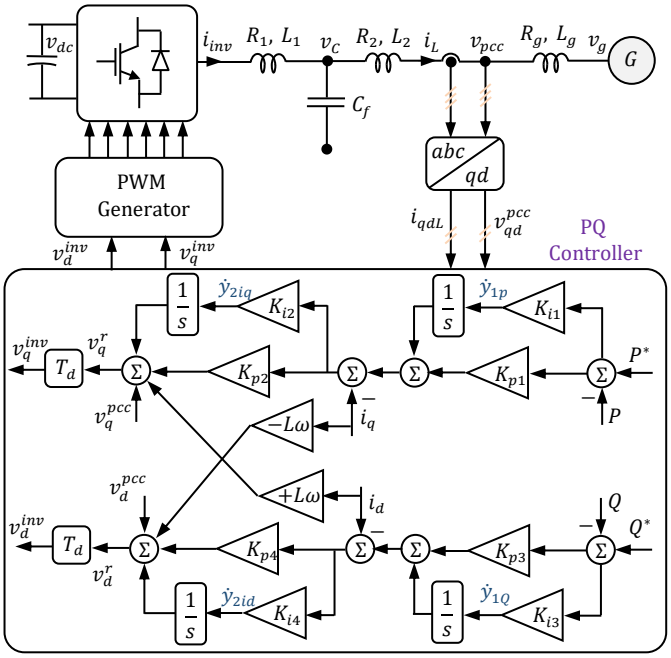

Fig. 1. A PQ controlled grid-following inverter (schematic diagram)

III. Online Grid Parameters Estimation Algorithm

This work implements two adaptive identification techniques: adaptive model reference and recursive least square methods to estimate unknown grid parameters. For the formulation of the online grid-parameter estimation techniques, one phase of a three-phase grid-interactive inverter is considered, as shown in Fig. 2. In literature, there are many active and passive methods [17] for grid parameter estimation, such as adaptive identification techniques, voltage transients, signal injections, etc. However, these methods cannot be directly applied for Z_g and V_g estimation because the grid voltage, V_g is unknown. Applying KVL at the PCC in Fig. 2, one can obtain the following equation

$$V_{pcc} = R_g i_g + L_g \frac{di_g}{dt} + V_g \tag{2}$$

In this work, a low-frequency signal injection method is utilized for estimating the grid parameters. This signal injection method introduces an external perturbation momentarily when new setpoints are received. Applying KVL at the PCC, one can calculate

$$\hat{V}_{pcc} = R_g \hat{\imath}_g + L_g \frac{d\hat{\imath}_g}{dt} \tag{3}$$

where, $\hat{\imath}_g$ represents the current injected into the grid at $f_{in} \neq 60\ Hz$ and $\hat{V}_{pcc}$ represents the measured voltage at the PCC at f_{in}. Notice, f_{in} is required to be chosen such that the grid voltage does not have any element at that frequency, i.e. $\hat{V}_g = 0$.

A. Recursive least square estimation method

This sub-section describes the RLS formulation for the Z_g estimation. The output measurement for the RLS, $y(t)$ at the time instant t_1 can be represented as

$$y(t_1) = \hat{\imath}_g(t_1), \tag{4}$$

and $u(t)$ is the input measurement for the RLS

$$u(t_1) = \hat{V}_{pcc}(t_1), \tag{5}$$

Consider T is the sampling time of the measurement and matrix $A = [a_1 \quad a_2]^{\mathrm{T}}$ which includes unknown parameters and measurement matrix $W = [-y(t_1) \quad u(t_1)]^{\mathrm{T}}$. The parameters can be expressed as $a_1 = \left(L_g T/R_g - 1\right)$ and $a_2 = T/L_g$. Therefore, the grid inductance can be represented as $L_g = T/a_2$ and grid resistance can be represented as $R_g = L_g T/(1 + a_1)$. In the recursive form, the least square problem is formulated using (5) and (6). Here, M is the number of measurements, R_M is the covariance matrix, where it is initialized as is 2×2

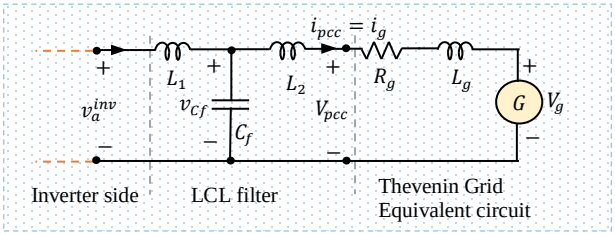

Fig.2. Simplified phase-a circuit of a three-phase grid-interactive VSI.

identity matrix, μ is the forgetting factor bounded as $\mu = [0\ 1]$ where μ is selected between 0.85 and 0.95. In addition, unknown parameter vector A can be estimated for M measurements as,

$$A_M = A_{M-1} - R_M^{-1} W(t_M)\big(W^T(t_M)A_{M-1} - y(t_M)\big), \quad (6)$$

where, the covariance matrix R_M is defined as

$$R_M = \mu \sum_{i=1}^{M-1} \mu^{M-i-1} W(t_i)W^T(t_i) + W(t_M)W^T(t_M), \quad (7)$$

Estimated R_g and L_g can be used to calculate the grid voltage using (1).

B. Model-reference adaptive estimation method

In addition to the recursive least square method, the parallel-series model-reference parameter estimation method is implemented to estimate the unknown grid parameter. The system block diagram of the parallel-series model-reference parameter estimation method is presented in Fig. 3. Similar to the recursive least square estimation method model reference estimation method can be applied for one of the line-line quantities presented in (1).

From (3), the unknown system parameters are defined as $a = -R_g/L_g$ and $b = 1/L_g$. Likewise, the adaptable reference model parameters can represent as $a_m = -R_{g,est}/L_{g,est}$ and $b_m = 1/L_{g,est}$. Thus, the discrepancy in parameter values can be calculated from $\Delta a = a - a_m = -R_g/L_g - (-R_{g,est}/L_{g,est})$ and $\Delta b = b - b_m = 1/L_g - \big(1/L_{g,est}\big)$. For accurate online estimation Δa and Δb should be reduced. Furthermore, the error in the state variable is required to be minimized to guarantee that the system and reference model is in good agreement. The dynamics of the error can be presented as follows,

$$\frac{d}{dt}e = (a_m - \beta)e + (a - a_m)\hat{\imath}_g + (b - b_m)\big(\hat{V}_{pcc}\big) \quad (8)$$

For the purpose of minimizing error, a proper positive definite Lyapunov function, V presented in (9) can be defined for the system described in (8). The Lyapunov function should be chosen such that $V \geq 0$ and $dV/dt < 0$. The Lyapunov function defined in (9) satisfied the requirements [24]-[27].

$$V = \frac{1}{2}\left(e^2 + \frac{1}{\gamma}\Delta a^2 + \frac{1}{\gamma}\Delta b^2\right) \quad (9)$$

where, $\gamma > 0$. The change in V with time can represent as the following,

$$\frac{d}{dt}V = e\frac{d}{dt}e + \frac{1}{\gamma}\Delta a\frac{d}{dt}\Delta a + \frac{1}{\gamma}\Delta b\frac{d}{dt}\Delta b \quad (10)$$

Substituting (8) into (10) results in

$$\frac{d}{dt}V = (a_m - \beta)e^2 + \Delta a\left(\hat{\imath}_g e + \frac{1}{\gamma}\frac{d}{dt}\Delta a\right) + \Delta b\left(e\big(\hat{V}_{pcc}\big) + \frac{1}{\gamma}\frac{d}{dt}\Delta b\right) \quad (11)$$

Based on (11), if $a_m < 0$, $e\hat{\imath}_g + (1/\gamma)\dot{\Delta a} = 0$, and $e\big(\hat{V}_{pcc}\big) + (1/\gamma)\dot{\Delta b} = 0$, then $\dot{V} \leq 0$. Thus, $\dot{\Delta a} = -(\gamma)e\hat{\imath}_g$ and $\dot{\Delta b} = -(\gamma)e(\hat{V}_{pcc})$. Consequently, we can write

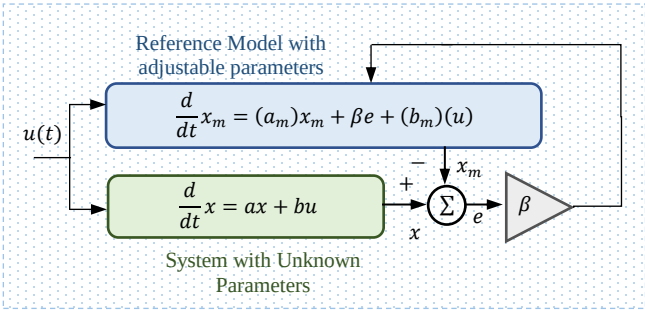

Fig. 3. General block-diagram of parallel-series model reference identification technique.

$$a_m = \gamma \int e(t)\hat{\imath}_g(t)dt$$
$$b_m = \gamma \int e(t)\big(\hat{V}_{pcc}\big)dt \quad (12)$$

Once b_m is estimated, the grid inductance $L_{g,est} = 1/b_m$. The grid resistance can be estimated from $R_{g,est} = -a_m/b_m = -a_m L_{g,est}$. The accuracy of the online estimation can be enhanced by choosing γ properly [28]-[30]. Then, the estimated grid parameters are sent to the self-protective reference model to adaptively check the validity of incoming power setpoints [15].

IV. Experimental Results

In this section, the performance of two grid-parameter estimation techniques are demonstrated experimentally using the hardware setup shown in Fig. 4. In this setup, a three-phase 5 kVA SiC MOSFET-based inverter is used, and the switching signals for the inverters are generated using the dSPACE MicroLabBox. In the experimental setup, the inverter feeds a 12 kW NHR 9410 power grid emulator through a three-phase LCL filter. Also, a programmable Magna-Power SL400-15/208 dc supply is used as input dc source for the inverter. The presented result in this section are recorded using Control Desk, a real-time software interface with dSPACE MicroLabBox, and then plotted using MATLAB. The experimental system parameters are $V_{LL,rms} = 208\,V$, $V_{dc} = 350\,V$, $L_g = 5\,mH$, $L_1 = 1\,mH$, $L_2 = 0.5\,mH$, $C_f(\Delta) = 27\,\mu F$, and $f_{PWM} = 20kHz$.

Fig. 5 shows the estimated grid inductance and resistance value using model reference adaptive and recursive-least square method. Both methods provide an almost similar precise result, see Fig. 4. Initially, the estimated grid inductance and grid resistance for both methods are approximately $5.5\,mH$ and $0.4177\,\Omega$, respectively. At $t = 22.12\,s$ additional $2.5\,mH$ is inserted, and the estimated grid inductance is $8.7\,mH$ with an error of 8.04%. For further demonstration of the accuracy of the two estimation methods, an additional $5\,mH$ is inserted at $t = 40.13\,s$. The estimated inductance value for this change is $15.01\,mH$, with an error of 15.38 %. It must be underlined that the resistance and inductance of the inserted inductor are functions of the current (power) flow temperature and proximity effects in the filter inductors. Therefore, the estimated inductance value is not precisely matching with the inserted value of inductance.

Two test scenarios are performed to demonstrate the impact of grid impedance on low-power hidden mode instability. In the first test scenario, the system initially runs when $L_g(= 2.5\ mH)$ and the setpoint is $P^* = 100\ W$ and $Q^* = 0\ Var$. Two active power setpoints, $P = 250$, and $P = 1200\ W$ are applied, and the dynamic responses are recorded from the dSPACE control desk, as shown in Fig. 6. For the applied setpoints ($P^* = 100\ W$, $250\ W$, and $1200\ W$), the dynamic responses are stable, see Fig. 6 (a). In the second test scenario, the inverter runs in a weak grid when $L_g(= 5\ mH)$, but for the same setpoints as the previous test scenario, the system has instability, see Fig. 6(b). When $P^* = 100\ W$, the system is stable. For $P^* = 250\ W$, the measured power fluctuates, and the system gradually becomes unstable. For $P^* = 1200\ W$, the system is stable again; see Fig. 6(b). Thus, an inverter can move from stable to unstable and unstable to stable depending on the setpoints and grid conditions [31]-[32]. These two experimental test outcomes are also in agreement with the stability analysis demonstrated in Fig. 7. For $L_g = 2.5\ mH$, the eigenvalues are located on the left-half plane, i.e., stable operation. On the other hand, for $L_g = 5\ mH$ at a low-power level, some of the

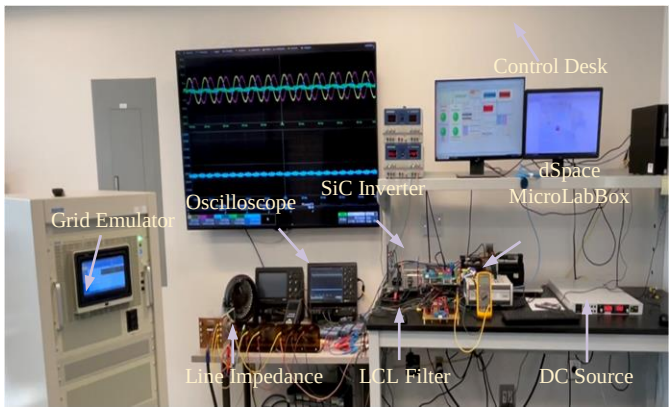

Fig. 4. Hardware setup for the 5 kVA three-phase grid-following inverter.

eigenvalues move on the right-half plane (unstable) and come back again to the left-half plane at a high-power level, see Fig. 7. Therefore, for weak grid conditions, i.e., high L_g, power setpoints can cause low-frequency instability for a certain range of power if the damping is insufficient in the system [33]-[34]. Therefore, grid parameters are required to estimate accurately so that the reference model can predict the dynamic responses for given setpoints.

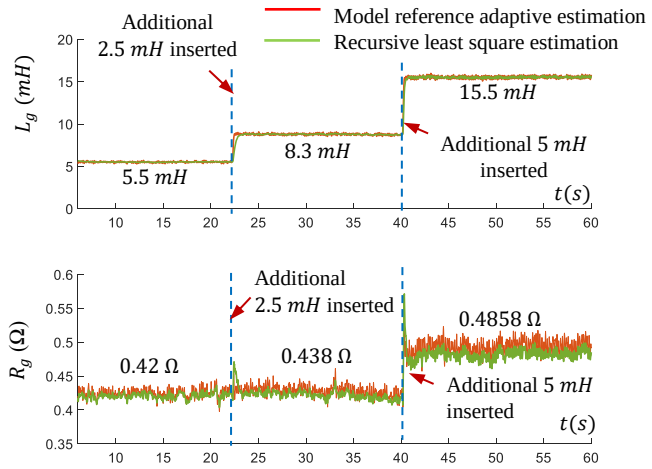

Fig.5. Estimated Thevenin grid-impedance using parallel-series model reference and recursive-least square estimation techniques

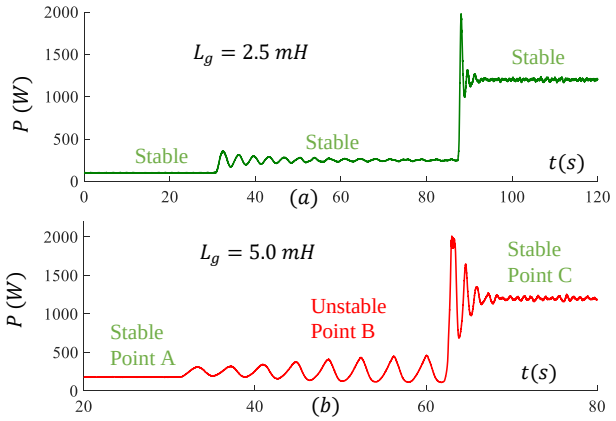

Fig.6. Experimentally obtained inverter's dynamic responses when the output power is changing step-by-step from 150 W to 400 W for (a) $L_g = 2.5\ mH$ (b) $L_g = 5\ mH$

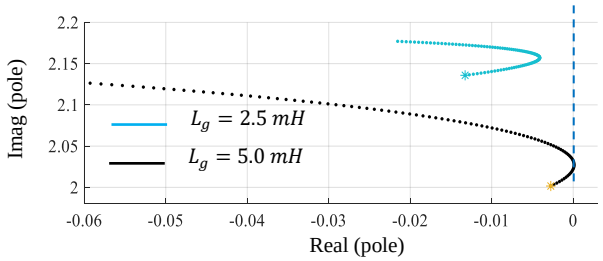

Fig. 6. A zoomed-in plot of dominant low-frequency positive eigenvalues using the full-order dynamic model as P is increased from 0.003 kW to 5 kW

To demonstrate the accuracy of the dynamic reference model, Points A and C was implemented 60 times, separately, and the statistics for the estimated location (real parts) of the dominant eigenvalues are plotted as shown in Fig. 8. Recursive

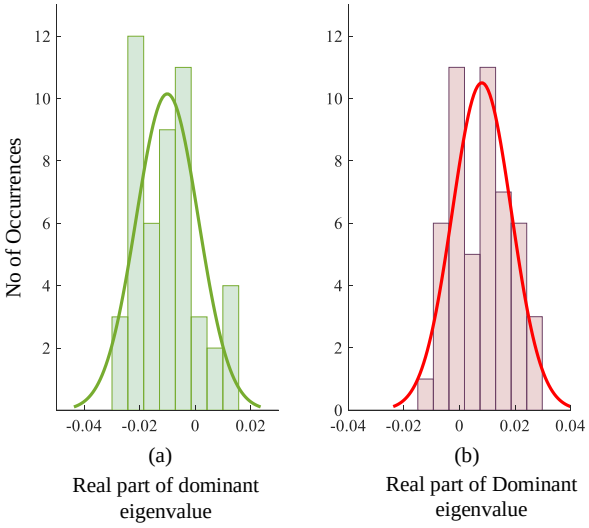

Fig. 8. Statistics of real part of dominant eigenvalues projection using reference model; (a) Active power change to 1200 W (Point C) from 100 W, (b) Active power change to 250 W (Point A) from 100 W.

least square method is implemented to estimate the grid parameters. Based on the number of occurrences, the μ and σ for the Point A are -0.01, and 0.011, respectively. For the Point C, the μ and σ are 0.0081 and 0.0106, respectively. Point A was predicted as a stable operating point with an accuracy of 85.6%, while Point C was predicted as unstable point with 78.5% accuracy. Therefore, the dynamic reference model is in good agreement with the actual cases.

V. Conclusion

This paper demonstrates the performance of the recursive-least square and model reference estimation method for online grid-parameter estimation. It has been found that with a combined signal injection method, both recursive least square and model reference adaptive estimation methods can estimate grid parameters accurately. Furthermore, this work also demonstrates that the inverter's reference model (full-order dynamic model) can project the dynamic response using the estimated grid parameters and protect the inverter from a harmful setpoint being engaged. This paper has experimentally verified the performance of the grid parameter estimation method and also experimentally and statistically validated the performance of the inverters' dynamic reference model.

References

[1] B. Mirafzal and A. Adib, "On grid-interactive smart inverters: features and advancements," *IEEE Access*, vol. 8, pp. 160526-160536, 2020.

[2] B. Arbab-Zavar, E. Palacios-Garcia, J. Vasquez and J. Guerrero, "Smart inverters for microgrid applications: a review", Energies, vol. 12, no. 5, Mar. 2019.

[3] M. Gursoy and B. Mirafzal, "On self-security of grid-interactive smart inverters," in Proc. IEEE Kansas Power and Energy Conference (KPEC), 2021, pp. 1-6.

[4] F. Sadeque and B. Mirafzal, "Frequency restoration of grid-forming inverters in pulse load and plug-in events," *IEEE J. Emerg. Sel. Top. Ind. Electron.*, pp. 1–8, 2022.

[5] M. Farrokhabadi *et al.*, "Microgrid stability definitions, analysis, and examples," *IEEE Trans. Power Syst.*, vol. 35, no. 1, pp. 13–29, 2020.

[6] D. Sharma, F. Sadeque, and B. Mirafzal, "Synchronization of inverters in grid forming mode," *IEEE Access*, vol. 10, pp. 41341–41351, 2022.

[7] M. Gursoy and B. Mirafzal, "Self-security for grid-interactive smart inverters using steady-state reference model," in *2021 IEEE 22nd Workshop on Control and Modelling of Power Electronics (COMPEL)*, 2021, pp. 1–5.

[8] J. Qi, A. Hahn, X. Lu, J. Wang and C. Liu, "Cybersecurity for distributed energy resources and smart inverters," IET Cyber-Physical Syst.: Theory Appl., vol. 1, no. 1, pp. 28-39, 12 2016.

[9] T. Hossen, F. Sadeque, M. Gursoy, and B. Mirafzal, "Self-secure inverters against malicious setpoints," in *2020 IEEE Electric Power and Energy Conference (EPEC)*, 2020, pp. 1–6.

[10] D. Saleem, A. Sundararajan, A. Sanghvi, J. Rivera, A. I. Sarwat and B. Kroposki, "A multidimensional holistic framework for the security of distributed energy and control systems," *IEEE Syst. J.*, vol. 14, no. 1, pp. 17-27, March 2020.

[11] Y. Wang, X. Wang, F. Blaabjerg, and Z. Chen, "Harmonic instability assessment using state-space modeling and participation analysis in inverter-fed power systems," *IEEE Trans. Ind. Electron.*, vol. 64, no. 1, pp. 806–816, 2017.

[12] Y. Xia, Y. Peng, P. Yang, Y. Li, and W. Wei, "Different influence of grid impedance on low- and high-frequency stability of PV generators," *IEEE Trans. Ind. Electron.*, vol. 66, no. 11, pp. 8498–8508, 2019.

[13] A. Adib, F. Fateh, and B. Mirafzal, "Smart inverter stability enhancement in weak grids using adaptive virtual-inductance," *IEEE Trans. Ind. Appl.*, vol. 57, no. 1, pp. 814–823, 2021.

[14] T. Hossen, M. Gursoy and B. Mirafzal, "Digital Twin for Self-Security of Smart Inverters," in Proc. 2021 *IEEE Energy Conversion Congress & Expo., 2021*, pp. 1-6.

[15] T. Hossen, M. Gursoy, and B. Mirafzal, "Self-protective inverters against malicious setpoints using analytical reference models," *IEEE J. Emerg. Sel. Top. Ind. Electron.*, vol. 3, no. 4, pp. 871–877, 2022.

[16] T. Hossen, D. Sharma, and B. Mirafzal, "Smart inverter twin model for anomaly detection," in *2021 IEEE 22nd Workshop on Control and Modelling of Power Electronics (COMPEL)*, 2021, pp. 1–6.

[17] P. Garcia,M. Sumner, A. Navarro-Rodriguez, J.M. Guerrero, and J. Garcia, "Observer-based pulsed signal injection for grid impedance estimation in three-phase systems," *IEEE Trans. Ind. Electron.*, vol. 65, no. 10, pp. 7888–7899, Oct. 2018.

[18] S. M. Abdelkader and D. J. Morrow, "Online thévenin equivalent determination considering system side changes and measurement errors," *IEEE Trans. Power Syst.*, vol. 30, no. 5, pp. 2716–2725, 2015

[19] D. Reigosa, F. Briz, C. B. Charro, P. Garcia, and J. M. Guerrero, "Active islanding detection using high-frequency signal injection*," IEEE Trans. Ind. Appl.*, vol. 48, no. 5, pp. 1588–1597, 2012.

[20] B. Arif, L. Tarisciotti, P. Zanchetta, J. C. Clare, and M. Degano, "Grid parameter estimation using model predictive direct power control," *IEEE Trans. Ind. Appl.*, vol. 51, no. 6, pp. 4614–4622, 2015.

[21] M. Ciobotaru, R. Teodorescu, P. Rodriguez, A. Timbus, and F. Blaabjerg, "Online grid impedance estimation for single-phase grid-connected systems using PQ variations," in *2007 IEEE Power Electronics Specialists Conference*, 2007, pp. 2306–2312.

[22] A. Adib, B. Mirafzal, X. Wang and F. Blaabjerg, "On stability of voltage source inverters in weak grids," *IEEE Access*, vol. 6, pp. 4427-4439, 2018.

[23] A. Adib and B. Mirafzal, "Virtual inductance for stable operation of grid-interactive voltage source inverters," IEEE Trans. Ind. Electron., vol. 66, no. 8, pp. 6002-6011, Aug. 2019.

[24] N. Cho, H.-S. Shin, Y. Kim, and A. Tsourdos, "Composite model reference adaptive control with parameter convergence under finite excitation," *IEEE Trans. Automat. Contr.*, vol. 63, no. 3, pp. 811–818, 2018.

[25] J. Benzaquen, F. Fateh, and B. Mirafzal, "On the dynamic performance of variable-frequency AC–DC converters," *IEEE trans. transp. electrif.*, vol. 6, no. 2, pp. 530–539, 2020.

[26] J. Benzaquen, F. Fateh, M. B. Shadmand, and B. Mirafzal, "One-step-ahead adaptive control scheme for active rectifiers in wild frequency applications," in *2019 IEEE Applied Power Electronics Conference and Exposition (APEC)*, 2019, pp. 588–593.

[27] A. Loria, E. Panteley, and M. Maghenem, "Strict lyapunov functions for model reference adaptive control: Application to Lagrangian systems," *IEEE Trans. Automat. Contr.*, vol. 64, no. 7, pp. 3040–3045, 2019.

[28] J. Benzaquen and B. Mirafzal, "An active rectifier fed by a variable-speed generator," in *2020 IEEE Applied Power Electronics Conference and Exposition (APEC)*, 2020, pp. 1691–1696.

[29] D. N. Gerasimov and V. O. Nikiforov, "Augmented error based adaptive control with improved parametric convergence," *IFAC-PapersOnLine*, vol. 55, no. 12, pp. 67–78, 2022.

[30] K. Guo, M. Li, W. Shi, and Y. Pan, "Adaptive tracking control of hydraulic systems with improved parameter convergence," *IEEE Trans. Ind. Electron.*, vol. 69, no. 7, pp. 7140–7150, 2022.

[31] T. Hossen, and B. Mirafzal, "On Stability of PQ-Controlled Grid-Following and Droop-Control Grid-Forming Inverters," in Proc. 2022 *IEEE Energy Conversion Congress & Expo., 2022*, pp. 1-6.

[32] A. Adib, F. Fateh, M. B. Shadmand, and B. Mirafzal, "A reduced-order technique for stability investigation of voltage source inverters," in *2018 IEEE Energy Conversion Congress and Exposition (ECCE)*, 2018, pp. 5351–5356.

[33] F. Sadeque and T. Hossen, "On control schemes of voltage source converters," *arXiv [eess.SY]*, 2021.

[34] T. Hossen and F. Sadeque, "On stability, ancillary services, operation, and security of smart inverters," *arXiv [eess.SY]*, 2021.